Experiments on Probing the Configuration Space of Post-Buckled Panels

D. Ehrhardt
Ehrhardt Engineering LLC,
Monticello, IL 61856
e-mail: ehrhardt.42@gmail.com

L. N. Virgin[1]
Department of Mechanical
Engineering and Materials Science,
Duke University,
Durham, NC 27708
e-mail: l.virgin@duke.edu

S. M. Spottswood
Structural Sciences Center,
Aerospace Systems Directorate,
Air Force Research Lab,
WPAFB, OH 45433
e-mail: stephen.spottswood.1@us.af.mil

This paper describes a primarily experimental study in which a nonlinear structural component (a slender, mechanically buckled panel) is subject to probing. That is, equilibrium configurations are explored when a specific location on the panel is subject to the application of a (variable) displacement constraint and characterized by a corresponding probe force. This probe force (in this study located at the center of the rectangular panels) is measured using a load cell and the resulting shape(s), taken up by the panel, measured using digital image correlation (DIC). Although the probe is only applied at a single location, this arrangement supplies considerable information about the changing equilibrium landscape including revealing co-existing equilibrium configurations using large perturbations and associated hysteresis phenomena. In addition, monitoring the probing force, and specifically when it drops to zero, provides a window into "free" equilibria that would otherwise be unstable and unobservable. Finally, it is shown that the probed equilibrium configurations provide the "landscape" within which any dynamically induced trajectories evolve including snap-through oscillations. [DOI: 10.1115/1.4048197]

Keywords: post-buckling, digital image correlation, potential energy, experimental mechanics

1 Introduction

The aerospace community needs greater understanding of the complex, post-buckled static and dynamic behavior of slender aerospace structures. This is especially true as analysts/designers pursue ever more efficient commercial air-vehicles with accompanying light-weight structural configurations. It is important to understand how these structures move between competing, stable equilibrium configurations while maintaining appropriate design margins, resulting in robust aerospace designs [1].

A nonlinear structure may possess multiple stable equilibrium configurations [2]. Under quasi-static but evolving loading conditions, the "natural" equilibrium path follows the route associated with a local minimum of the underlying potential energy. The path is robust against small perturbations, at least until buckling occurs, and the local potential minimum is lost. In nominally symmetric systems, for example, the classic Euler column [3], there is typically a post-critical pair of paths emanating from the initially trivial (undeformed) state, i.e., the stability transition is classified as a supercritical pitchfork bifurcation [4]. Which path is followed depends on any inevitable (small) bias, initial imperfection, or indeed any parameter that has a tendency to break symmetry and can be difficult to predict in a practical situation. However, once this post-buckled regime is entered, there are still two (near-symmetric) stable equilibria, even though only one path can be followed under the smooth change in a control parameter. Locations on the "other" path, the road not taken, can be viewed as remote equilibria. Therefore, under *fixed* post-buckled axial loading conditions, it is possible to perturb between these two equilibria, *providing the perturbation is large enough*. This is the focus of the current paper: experimental determination of equilibrium states (both stable and unstable) by probing the configuration space. Other approaches to the experimental determination of unstable equilibria can be found in Refs. [5–10].

Consider the scenarios illustrated in Fig. 1. They all appear to be quite similar—near straight beams in equilibrium (initially unloaded), with fixed boundary conditions, and then subject to a lateral load. In part (a), we have a beam that undergoes a *unique* deflection under loading, with a linear stiffness; in part (b) a beam with a non-straight equilibrium configuration is subject to a lateral force *in the direction* of the initial shape, and again the subsequent deflection is unique and predominantly linear. However, in part (c), we apply the load in the *opposite* direction to the initial shape, and now subsequent deflection can suddenly pop-through to an inverted equilibrium configuration (shown by the dashed line), clearly a nonlinear situation [11]. In part (*d*), we have an initial shape that is somewhat "deeper" than that in part (*c*), and now a lateral load will typically result in marked asymmetric behavior (characterized by the angle θ in Figs. 1 and 2, but later simply using separated lateral displacements) during the transition to the snapped-through shape. The multiple stable equilibria in parts (*c*) and (*d*) must be accompanied by unstable equilibria, and these are indicated by the grey (red) lines.

Each of these shapes represent an equilibrium configuration: some stable (associated with a minimum of the underlying potential energy) and some unstable (also associated with turning points in

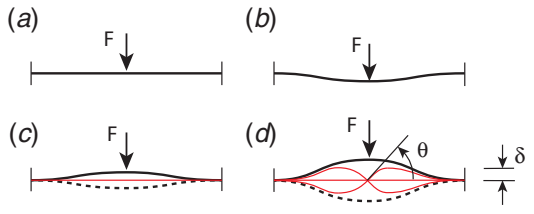

Fig. 1 Laterally loaded slender structures and the influence of initial curvature. The black lines show stable equilibria: continuous—initial shape; dashed lines—a "remote" equilibrium shape. The grey (red) lines show possible unstable equilibria when *F* drops to zero during the transition between stable states. (Color version online.)

[1]Corresponding author.

Contributed by the Applied Mechanics Division of ASME for publication in the Journal of Applied Mechanics. Manuscript received April 19, 2020; final manuscript received August 11, 2020; published online September 16, 2020. Assoc. Editor: Pedro Reis.

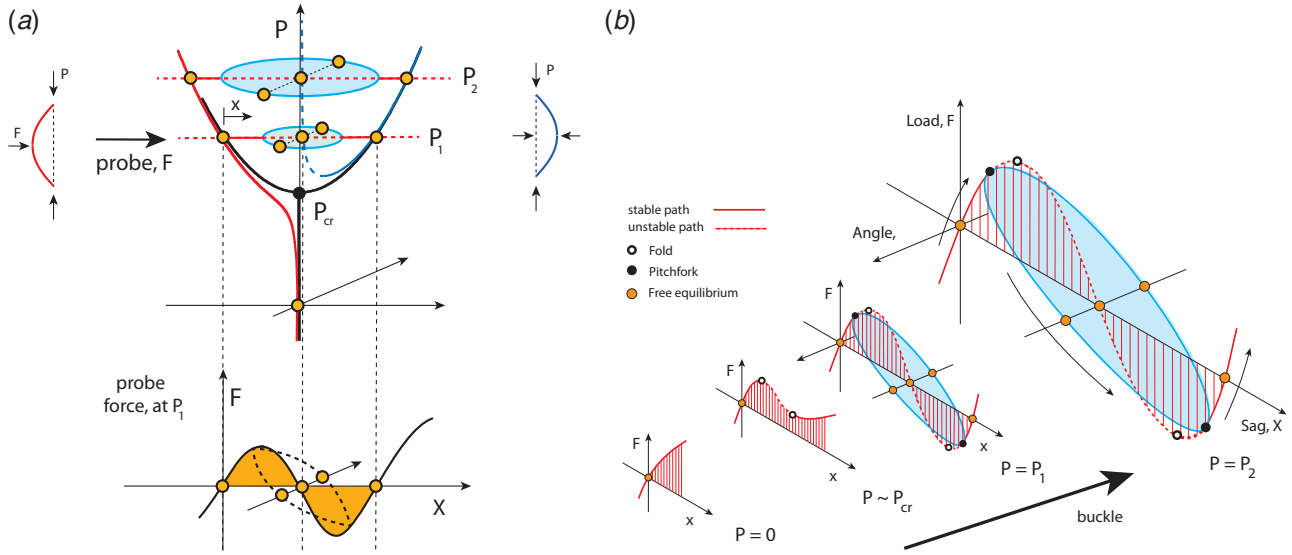

Fig. 2 (*a*) A typical example of nominally symmetric buckling (a super-critical pitchfork bifurcation), producing co-existing post-critical non-trivial equilibria and (*b*) typical (probing) equilibrium paths with the appearance of a second (asymmetric) degree-of-freedom as buckling progresses

the underlying potential energy, but now at least one dimension has a negative curvature). These (free) equilibria correspond to effectively unloaded states when ($F \to 0$), and would feature in the measurement of F under increasing or decreasing conditions. In part (*c*), we would expect F to increase (a positive stiffness) and then drop to zero at the straight (red/grey) configuration, followed by a negative force that also curves back to zero for the complementary stable equilibrium configuration (dashed line). We observe that in part (*d*), there are essentially two degrees- of-freedom (an angle in addition to the vertical deflection), and thus, strictly speaking, we would also require a zero torque to display the equilibria. In this sense, a degree-of-freedom can be constrained and the corresponding force required gives *some* information about features of the configuration space, and hence the underlying potential energy. Clearly, this is a much more challenging scenario in higher-dimensional spaces.

Suppose we fix a system in a stable equilibrium configuration that is not unique, e.g., in parts (*c*) and (*d*) of Fig. 1. In a conventional experimental scenario, i.e., under conditions of dead loading for example, the path follows the stable equilibria only. But suppose we attach a load cell to the structure, such that moving the structure (at the point of attachment) requires a pushing, or pulling, force that is measured. Under these conditions, we can seek to identify equilibria, including those that are unstable (when the probe force F drops to zero), e.g., saddle-points. We shall initially focus on the type of situation described in part (*d*), that is, an identification of probing force to extract equilibria in which there are two dominant modes of deflection (a translation δ and a rotation θ). The specific structures chosen are thin rectangular plates, a prime example of super-critical pitchfork bifurcational behavior and a form of important practical application and intense previous studies [12–20]. Under various degrees of post-buckling, we shall examine the evolution of certain characteristic "buckled" shapes due to probing. The unstable equilibria play an important role in estimating the global robustness of a given configuration as well as strongly influencing large deflection dynamic behavior, a major concern in sonic fatigue, for example, Refs. [21–24]. Highly nonlinear structures with perhaps many active degrees-of-freedom present significant challenges, with the current approach considering a somewhat limited view based on probing at a specific spatial location.

1.1 Post-Buckling. One of the natural ways in which the above scenario occurs is via the process of stable-symmetric buckling [4]. As an axial load P is increased, the initial trivial (straight configuration) loses stability and results in two stable equilibria, which can be thought of as buckled "in" and buckled "out" (see Fig. 2(*a*)). If we next introduce an applied lateral load F at a fixed level of P, we essentially obtain the scenarios described in Fig. 1(*d*), with P identified as the control parameter that determines the initial buckled shape.

Suppose we load a slender structure to level P_1, as shown in Fig. 2(*a*). The structure sits naturally in a configuration characterized by $(P, -\delta)$. We then apply the probe force F in this direction and introduce an incremental coordinate X (in the δ-direction), measured from equilibrium. As the load cell is moved in the X-direction the corresponding force follows the path shown schematically in the lower part of Fig. 2(*a*). Each time the probe force passes through zero corresponds to equilibrium. And we see the possibility of equilibria in another mode (characterized by an angle θ, and away from the δ axis in this example). Figure 2(*b*) also shows this scenario, in which the probe initially causes a symmetric deflection (in X only), but then a (pitchfork) bifurcation occurs and deflection grows in an asymmetric mode. Upon subsequent increase in the lateral probe position the force traces out configuration shapes with a subsequent return to symmetry as the system enters its fully snapped-through configuration. In this way, we monitor (probe), the force-deflection relation at different axial loading levels with a specific focus on where the force drops to zero. For example, at force level P_2, the structure is more buckled with correspondingly greater deflection. We assume this situation is entirely elastic, i.e., very slender structures, but by no means path-independent, since conducting a reverse sweep would result in an eventual return to the initial equilibrium configuration but with the possibility of hysteresis.

The extent of the buckled configuration is broadly related to the lateral force required to deflect the panel into a given shape. That is, we elastically bend a panel from an initially flat shape and then clamp it at the edges to maintain a deflected configuration that we refer to as "buckled." In an experimental context, clamping in a deflected configuration is easier to accomplish than maintaining a fixed axial load, including thermal loading, say [25]. That is, the panel under initially loose boundary conditions is pushed with a lateral side-force and then clamped at the perimeter to stay in that configuration. The greater the initial lateral force, the greater the initial deflected configuration. Some approximate analysis relevant to the initial shapes can be found in the Appendix. For a mildly buckled (almost flat) structure, the probing would result in symmetric snap-

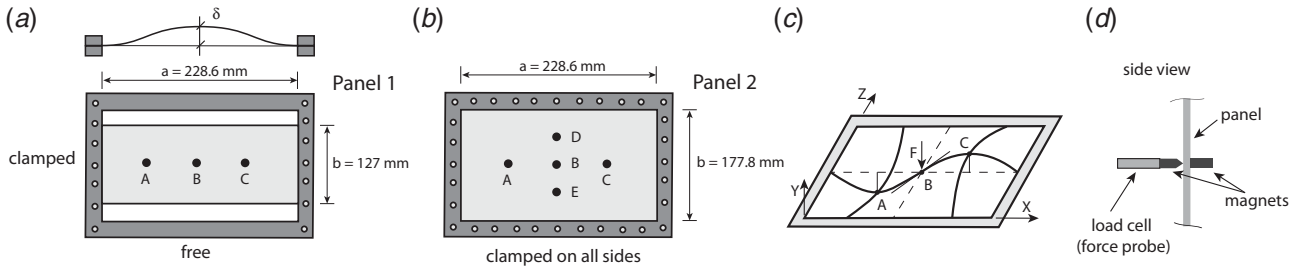

Fig. 3 The two panel geometries under consideration, (*a*) Panel 1, (*b*) Panel 2, (*c*) a typical deflection shape. The asymmetry about the center is based on $(Y_A - Y_C)/(X_A - X_C)$ or $(Y_D - Y_E)/(Z_D - Z_E)$ for asymmetry in the X- and Z-directions, respectively, (*d*) detail of the force probe application.

through, sometimes termed a fold, and characterized by a single mode, but in general, the complexity increases with nonlinearity.

2 The Specific Panels

We shall focus on two panels, both made of 0.508 mm thick aluminum (2024-T4):

- Panel 1: Clamped-free (on opposite edges), aspect ratio $a/b = 228.6\,\text{mm}/127\,\text{mm} = 1.8$.
- Panel 2: Fully clamped (on all four sides), aspect ratio $a/b = 228.6\,\text{mm}/177.8\,\text{mm} = 1.286$.

These are shown schematically in Fig. 3.

Both panels are relatively slender with $a/d \approx 400$ (d is the thickness) and relatively easily pushed into a deformed shape (elastically), with δ (later to be identified with Y), typically on the order of a few millimeters.

It is interesting to note the relation between mid-length lateral, δ, and axial deflection, ϵ, (assuming inextensibility). For a mildly buckled column, it can be shown that the relation between these two is given by $\Delta L = \epsilon = -1/2\int_0^L (dy/dx)^2 dx$ and given boundary conditions fixed against lateral deflection and rotation, this leads to $\delta/L \approx (2/\pi)\sqrt{\epsilon/L}$. Thus, it only takes a relatively small axial deflection to cause the buckling relevant to the current study. In any case, a central lateral point load is applied to the panels with relaxed (in-plane) boundary conditions and then clamped in place. Such a state then defines an initial "free" equilibrium configuration, i.e., one of the continuous black lines in Fig. 2, about which probing is initiated. The initial buckled shape could have just as easily been obtained in the opposite direction. However, this alternative equilibrium configuration (close to a mirror image) is still present, separated from the initial equilibrium configuration by unstable configuration(s). Probing causes the system to pass through (interrogate) the potential energy landscape, and it is the monitoring of the probing force and corresponding panel deflected shape, and what this tells us, that is the primary focus of this paper.

3 Experiment Setup

The two panel geometries were setup in a rigid frame in the lab, as shown in Fig. 4. The panels were first loosely installed in the frame and then each panel was laterally deflected to varying extents (governed by the approximate linear behavior described in the Appendix), clamped uniformly around the perimeter to a pre-determined and consistent torque of 81 Nm, and rigidly attached to the stiff loading frame.

The digital image correlation (DIC) system was used to measure the full-field initial (buckled) shape and its snapped-through configuration.

The linear displacement controller was then incremented to push the load cell (via a conical steel tip) onto the center of the panel. Snap-shots of the deflected shape were taken at small increments of the corresponding load. Small, powerful magnets, (cylindrical and conical rare-earth magnets of about 12 mm in diameter) sufficiently strong to maintain contact between the panel and the tip of the load cell were used on the backside of the panel (opposite to the load cell tip), allowing the load cell to pull-back on the panel and record negative load values (see Fig. 3(*d*)). An alternative to this could involve either attaching the load cell (stinger) to the panel, or applying a load cell to both sides, however, both of these approaches had their practical drawbacks. Even for the least buckled shape, it was apparent that some asymmetric behavior occurred. Whenever this occurred, the panel was manually pushed through to the mirror-image asymmetric shape, and data recorded as the load cell moved forward and backward, and under further large perturbations in order to explore the configuration space. The choice of magnets was based on trial and error, with a variety of magnet shapes, e.g., a "bullet"-shaped tip was used to

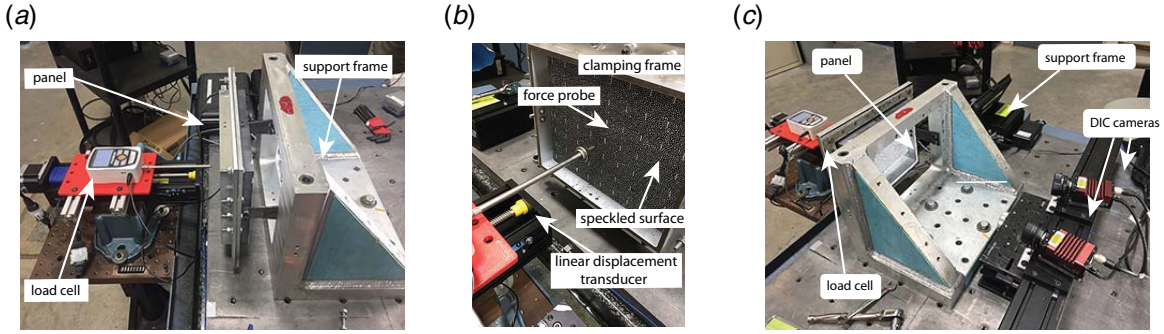

Fig. 4 Overall views of the experimental setup, showing (*a*) the digital force gage mounted on a linear bearing displacement control, (*b*) the speckled panel, and (*c*) the DIC cameras

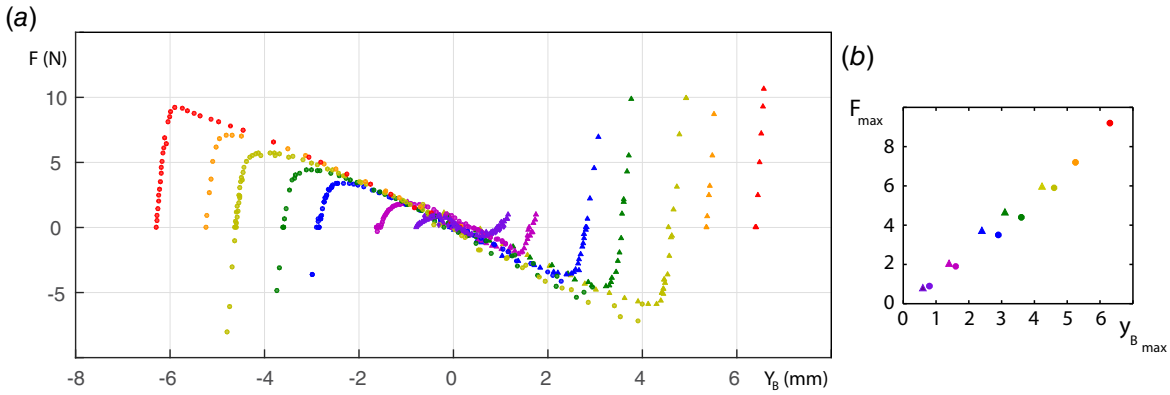

Fig. 5 (*a*) Probe force versus displacement at the plate center for various degrees of initial deformation and (*b*) maximum load carrying capacity (snap under force control) versus corresponding deflection (measured from flat). In this and later figures, the circle and triangle symbols correspond to the direction of probing, and to help differentiate between loading paths.

reduce any constraint on rotation at the probing point, or "flat-faced'-shaped magnets used to constrain rotation in order to explore (unstable) symmetric equilibrium paths although this was only achieved for the smallest buckled configuration due to the much higher strain energy associated with those paths. For these panels with greater initial deflection, the equilibrium path followed the asymmetric one denoted in Fig. 2(*b*) (see pitchfork bifurcation).

The panels were speckled with a randomized black/white pattern, based on previous studies. Full-field deflection shapes at every level of probing were measured using the cameras shown in Fig. 4(*c*)—a quasi-static 3D-DIC system composed of two Allied 6MP (2752 pixels × 2200 pixels) CCD cameras. A calibration target was used to determine a calibration deviation of 0.021 pixels or 0.0023 mm. Images were individually triggered with a shutter speed of 1/15 s. Deflections in 3D at each deformed state were computed with the commercial digital image correlation software ARAMIS and post-processing using MATLAB.

4 Experimental Results

4.1 Panel 1: The Clamped-Free Panel. The first step in the experimental procedure is to deflect the panel into an elastically deformed shape(s) with relatively loose boundary conditions, prior to clamping. Using the approximate beam theory in the Appendix (and bearing in mind that the boundary conditions are quite fixed, out of plane), and assuming the panels are initially flat, if we apply a lateral central point force, we would expect a corresponding central lateral deflection roughly according to the linear theory in the Appendix. The lateral load was measured with the digital load cell. For loads of $F_0 = 1.8, 2.8, 5, 7.1$, and 10 N, we would expect corresponding initial central deflections in the vicinity of $Y_B \approx 1.0$, 1.6, 3.1, 4.0, and 5.7 mm, based on the *linear* theory $F_0 = 1.76\, Y_B$ from the Appendix, i.e., the linear lateral stiffness is $E\, d^3/(0.1\, a^2) = 1.76$ N/mm. These approximate values were used in order to provide a broad spread of "buckled-shapes" to be probed, i.e., both F_0, and P (in the introduction) govern the degree of initial deformation, although they then play no further role in the study. It is also likely that the nonlinear membrane effect would start to influence (increase) the stiffness for these relatively large deformations.

Figure 5 shows a summary of the experimental data for panel 1 under various degrees of initial buckled shapes. Here, although "F" is still a lateral, central point load, it is now designated as a measure of the probe load applied to the already deformed shape (in the opposite direction to the original F_0). The deflection, Y_B, is measured at the geometric center of the panel, and this has been shifted in each case so that the origin corresponds to the nominally flat (unloaded) configuration.

Part (*b*) shows a plot of the maximum load (at which a snap instability would occur under conditions of force-loading). Clearly, the greater the initial extent of buckling, the greater the lateral force needed to push the system to snap-through, and this relation is nearly linear. In this plot the deflection is measured from the flat panel, which under the buckled condition is highly unstable. Interestingly, as a function of deflection measured from the buckled state itself, the additional deflection prior to buckling is somewhat independent of the degree of buckling. As will be seen a little later, the snap-buckling is initiated by asymmetric bifurcation where the deflection is characterized by a marked angular component. The slight, but inevitable, asymmetry in the unloaded panel results in the slightly different buckling loads when loading from each side.

From the $F = 0$ intercept of the data in Fig. 5, we see that the initial buckled amplitudes are relatively close to the values predicted by linear theory (discussed in the Appendix), especially given the imprecise theory and boundary conditions (prior to clamping). Initially, the panels are relatively stiff, but then a pitchfork bifurcation is encountered and the load starts to (suddenly) decline. The sudden change in the vicinity of the maximum load is an artifact of projection. That is, at the bifurcation, the panel starts to deform asymmetrically (out of the plane of the figure). However, since the full-field is measured with DIC, we can approximate the

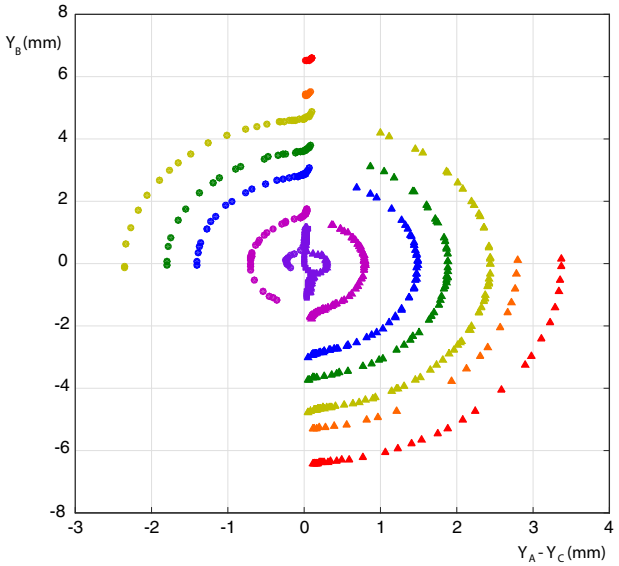

Fig. 6 A measure of asymmetry in the response, plotting the lateral deflection on either side of the (horizontal) centerline

central angle (and hence asymmetry) by using the deflection of the quarter-points Y_A and Y_C, say, with their locations shown in Fig. 3.

Plotting the difference between these two deflections $Y_A - Y_C$ against Y_B gives the results shown in Fig. 6. The force axis is into the page, with initial data in this direction as the center of the panel deflects symmetrically at first (with $Y_A - Y_C \approx 0$). After a range of asymmetric deformation the behavior returns to a symmetric shape as the probe pushes through to the remote free equilibrium, and beyond. It is interesting to note that there is a small jump in the response as the system snaps back to the symmetric response, and this may be partly attributed to any small off-center aspect to the probe, and an inevitable bias in the initial symmetry of the equilibria. We also note that for the panel under the mildest buckled condition, the magnets attaching the load cell to the panel were sufficiently strong (relative to the probe loading) that it was possible to follow the symmetric path (which would ordinarily be unstable) along its length by suppressing the angle at the center. Data were not acquired for the larger buckled configurations under "pulling" conditions due to the limited strength of the magnet.

For a more complete picture, we plot both the symmetric and asymmetric deflections versus lateral load in Fig. 7.

This provides a real-data version of the schematic behavior shown in Fig. 2.

4.1.1 Panel Shapes Under Load. As mentioned, the DIC system provides a powerful full-field, non-contacting tool for measuring the complete deflected shape. We provide samples of the typical deflection shapes here, and corresponding to the probing of the lowest initial buckled state as shown in an expanded view in Fig. 8(*a*).

Figures 8(*b*) and 8(*c*) show examples of the two forms that dominate the behavior, plus an additional shape that was possible (part *d*). They can be identified with specific points in the load-deflection space by the symbols as indicated in the key. In part (*b*), we observe a symmetrical shape corresponding to the initial equilibrium configuration, and representative of the deformed shape under small increasing probe loading, i.e., the "natural" loading path. Part (*c*) shows the asymmetrical shape resulting from a bifurcation and can be thought of as a second mode-type shape (with a significant angle near the panel center). Part (*d*) shows a deformed shape in which the asymmetry is in the vertical orientation. In each, we might anticipate a corresponding "mirror-image" shape. For example, the shape in part (*b*) can be thought of as buckled-in, with a remote snapped-through buckled-out shape present. As mentioned earlier, these boundary conditions lead to a panel that is not significantly different from a beam or shallow arch, with the two shapes shown in Figs. 8(*b*) and 8(*c*) dominating behavior.

4.2 Panel 2: A Clamped-Clamped Panel. This section describes some probing experiments conducted on a thin panel, clamped on all four sides. Since the same support frame used in the previous section was re-used, the aspect ratio became 9:7 (it was 9:5 for panel 1), with essentially the same procedure followed, i.e., deflecting the panel to various extents prior to clamping and then investigating the possible configuration under an applied constraint at the geometric center of the panel.

In this section, we subject the panel to three different levels of deflection prior to clamping (buckling extent). Given the increased complexity of possible behavior, we start by listing the typical shapes to be encountered, and consider each buckled panel separately. Again the deflection is shifted such that the origin corresponds to the flat panel. Shown in Fig. 9 are representative shapes observed under central point loading.

4.2.1 The Mildly-Buckled Case. Initially, the panel was placed loosely in the support frame and then deformed prior to clamping, such that the central lateral deflection, and its snapped through mirror-image, were in the range 0.80–0.83 mm, i.e., about one and a half the panel thickness (0.508 mm). The centrally loaded probe (the load cell) was again used to explore possible configurations under a displacement constraint at the center of the panel, as shown in Fig. 10(*a*). For this case, the panel transitioned from the positive symmetrical buckled shape 1 (shown in Fig. 9(*b*)) to the negative symmetrical shape 1 through the asymmetrical shape 2 (Fig. 9(*c*)). At the second zero crossing in the force-deflection curve shown in Fig. 10, only a single branch of the asymmetrical shape 2 was found.

This mildly-buckled case is closest to panel 1 and confirms the dominance of the first two shapes (1 and 2).

4.2.2 The Moderately Buckled Case. The panel was then loosened at the boundary, again elastically deformed (but to a greater extent) and re-clamped, with a "buckled" amplitude(s) of about 1.1 mm or roughly twice the panel thickness. The force-deflection curve, Fig. 11(*a*), is color coded to show the presence of two curves: blue (dark grey) corresponds to the primary buckling branch including a transition from the symmetrical shape 1 to the asymmetrical shape 2 and red (light grey) corresponds to a jump to the asymmetrical shape 3. For visual clarity, in this plot (and subsequently), the data is projected onto the buckled shapes: $q = \Phi z$, where $\Phi_{m\times n}$ is a matrix of m buckled shapes (with $F = 0$), and $z_{n\times 1}$ is a vector of measured deformation at n points, with Φ scaled to unity (giving units of millimeters). There are four distinct regions shown in Fig. 11(*b*) and emphasized with marker type: circles correspond to the positive primary buckling branch, squares to the negative, triangles to the asymmetrical shape 3, and

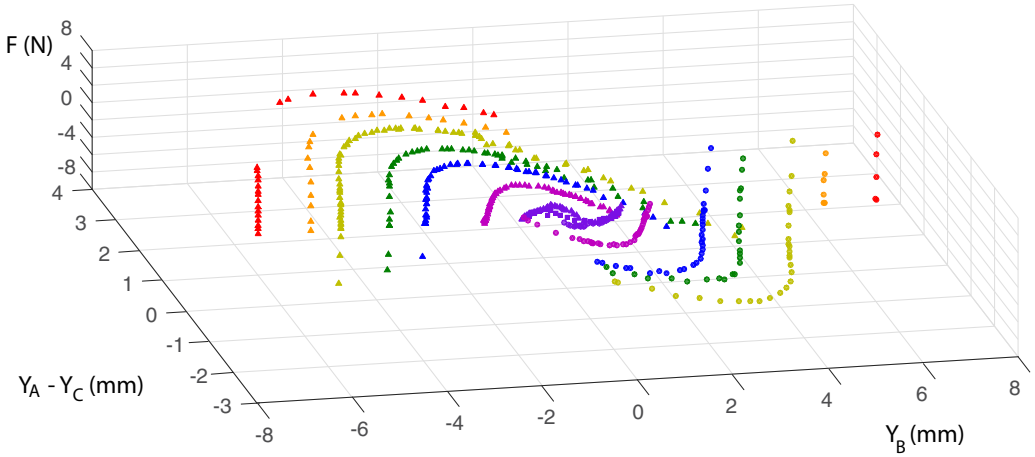

Fig. 7 A 3D view of the load deflection characteristics for the clamped-free panel under various degrees of initial deformation

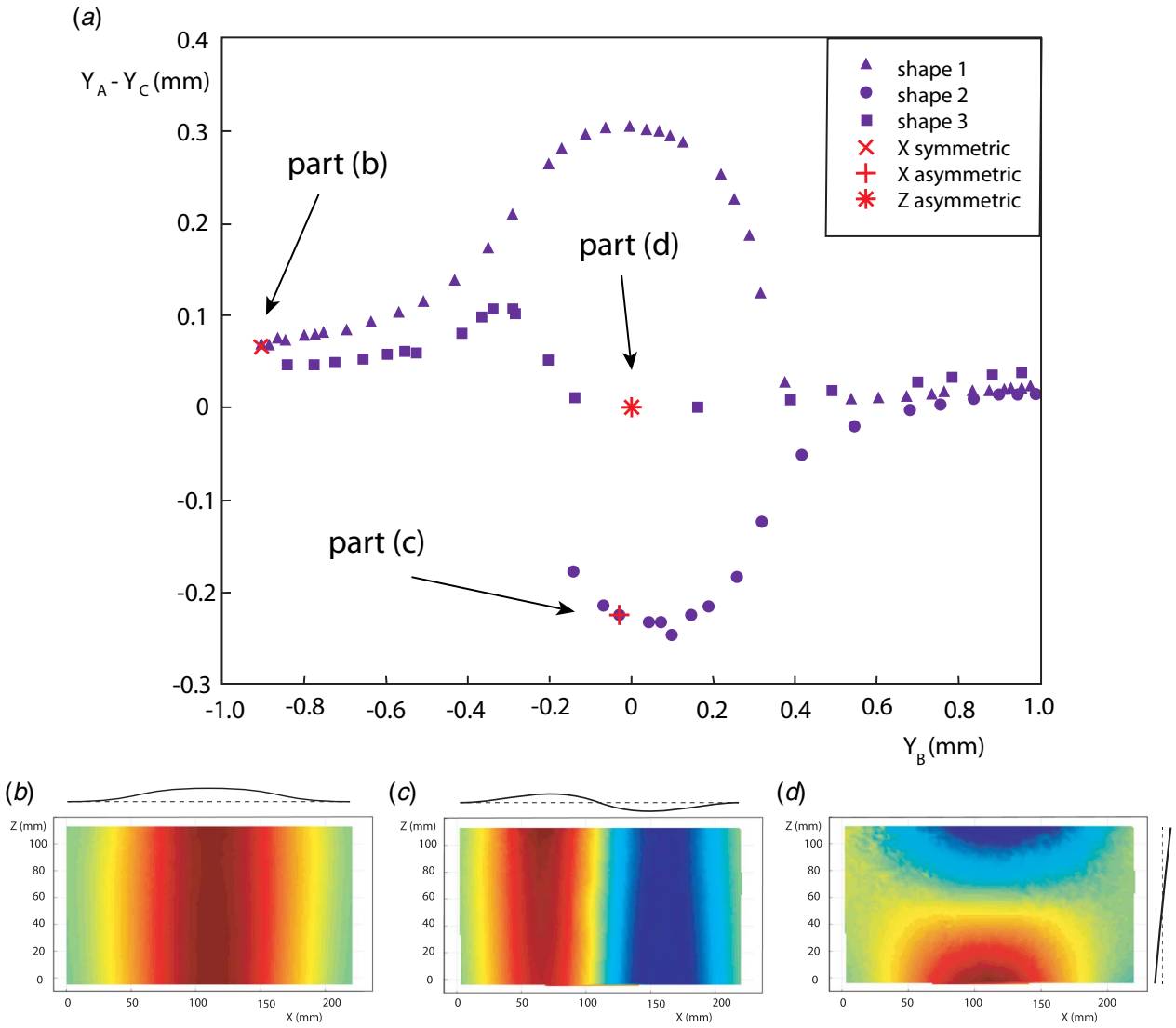

Fig. 8 Typical deflection shapes under lateral loading: (*a*) the load-deflection relation, with three identifiable paths, (*b*) symmetrical; shape 1, (*c*) asymmetrical; shape 2, and (*d*) a shape with a marked asymmetry in the Y-direction; shape 3

inverted triangles to the asymmetrical shape 3 inverted along the Z center-line of the panel. In this case, we have superimposed some of the data from the mirror-image responses. A number of equilibrium paths can be followed, and these paths may include discrete jumps, and the application of large perturbations can be used to cause a transition between them. All branches were reached multiple times throughout testing, leading to the conclusion that this is a product of buckling level and not just the experimental setup. The convoluted nature of the paths illustrate that under nominally fixed (force) conditions, the panel may exhibit a variety of co-existing stable equilibrium shapes.

4.2.3 A More Heavily Buckled Case. Finally, the panel was subject to a relatively high lateral force prior to clamping. The "buckled" amplitude was about 1.72 mm or about three times the panel thickness.

In this case, and not dissimilar to a *deep* arch, the force-deflection behavior is more complicated. Figure 12(*a*) shows the force-deflection projected onto the initial shape (q_1). After the initially growing symmetric shape the system undergoes a number of branch switches, some of which involve sudden jumps. This is also the case for a reversal of the loading. The data points in Fig. 12 thus present a necessarily severe projection from a relatively higher-order space. This space is spanned by the shapes shown in Fig. 9 including some mirror images. For discussion, the higher order buckling shapes are plotted versus the first buckled shape in Figs. 12(*b*)–12(*d*). The plots are color coded as follows: blue (shape 1), red (shape 2), magenta (shape 3), and light blue (shape 4). The force deflection (Fig. 12(*a*)) curve shows the transition from positive shape 1 to negative shape 1 through several buckling transitions. A closer examination of Fig. 12(*b*) clearly shows an isolated location of shape 2 through this transition. The deflection path following shape 3 is the most complex as seen in all plots in Fig. 12. In each plot, groupings of shape 3 deflections represent coupling between shape 3 and all other shapes. Finally, the deflections corresponding to shape 4 are shown as continuations of shape 1 in Fig. 12(*d*). The complexity of the possible stable equilibrium states under lateral force probing for this level of buckling is striking.

5 Dynamic Response

This paper has focused on the mechanics of a classical bi-stable system, in which equilibrium configurations could be accessed by probing with a quasi-static force, in this case at the center of the panel. Probing can also be accomplished by pushing (or pulling)

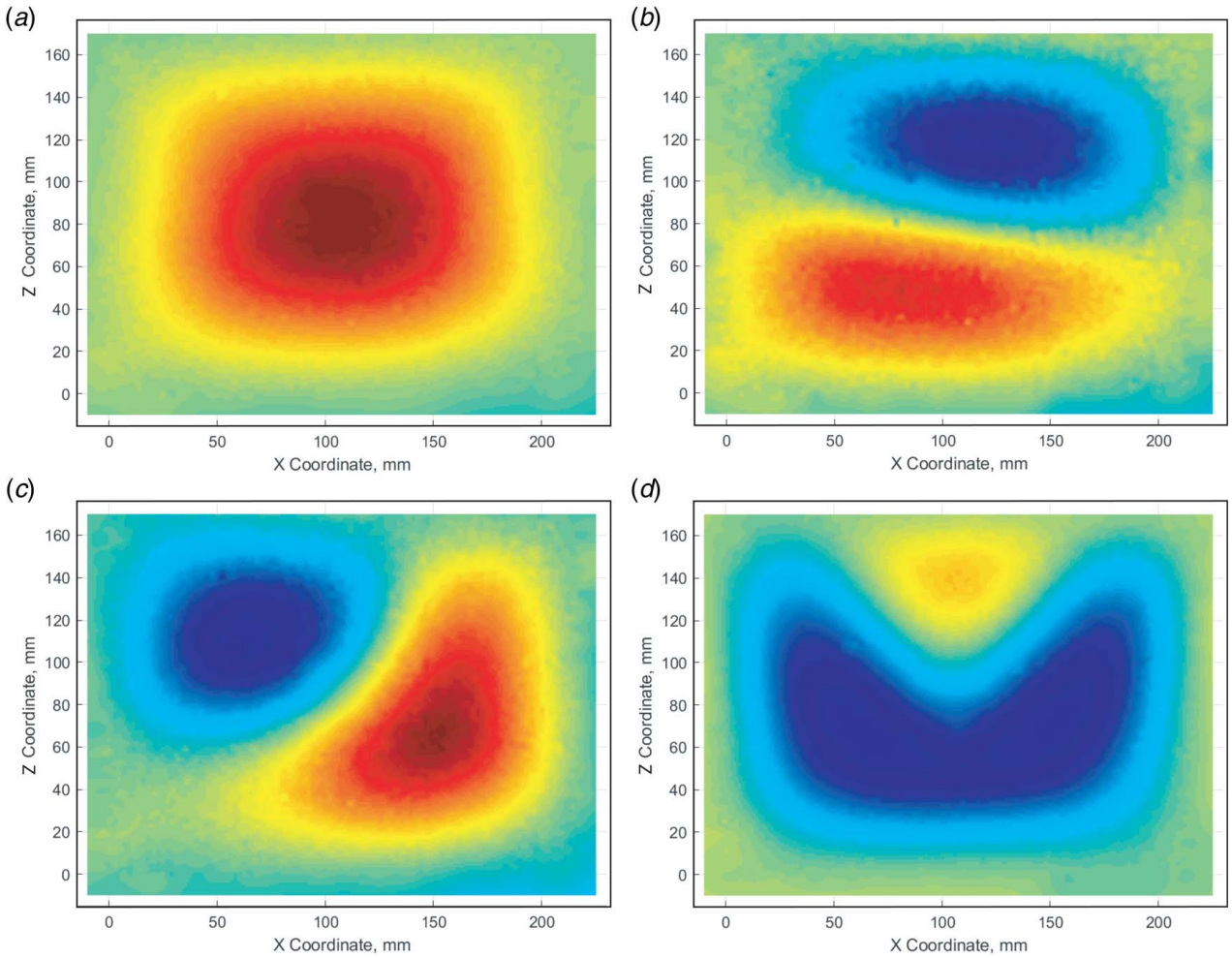

Fig. 9 Typical deflection shapes under lateral loading: (*a*) symmetrical: shape 1, (*b*) asymmetrical; shape 2, (c) asymmetrical; shape 3, and (*d*) shape 4.

at any location on the panel. Alternatively, if the panel is subject to dynamic excitation, the forces generated might be sufficient to cause the panel to move (dynamically) through an equilibrium landscape that is dominated by various stable (and unstable) equilibrium configurations.

To give a specific example, we return to a mildly buckled case, in which the clamped-free panel is subject to a lateral load of approximately 2.5 N and then clamped in place. That is, broadly corresponding to the magenta static results in Fig. 6. The complete testing system (the panel and its support structure) was then placed

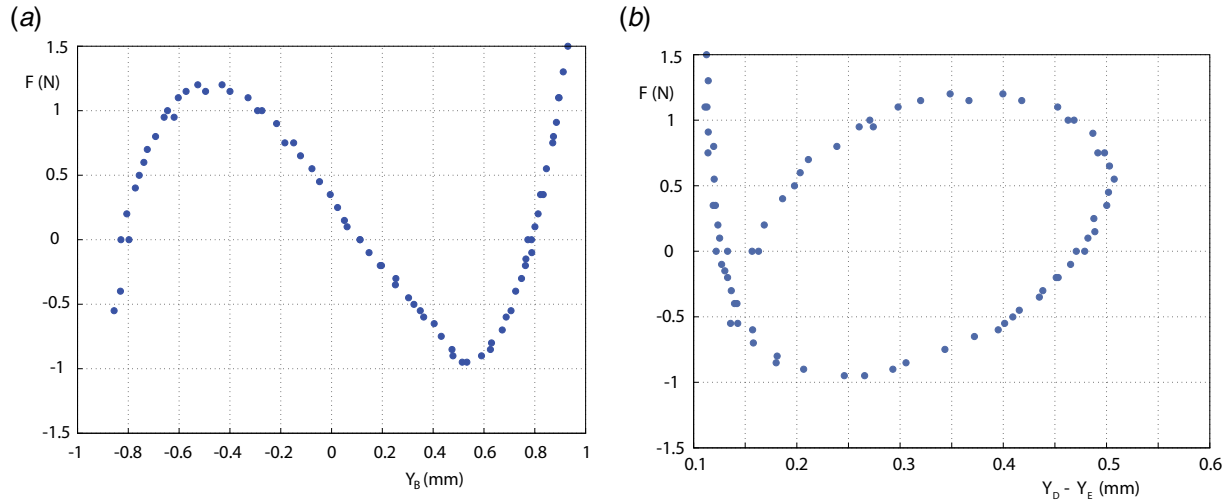

Fig. 10 Deflection as a function of probe force, mildly-buckled: (*a*) force versus center deflection and (*b*) force versus difference between Y quarter points in the Z-direction.

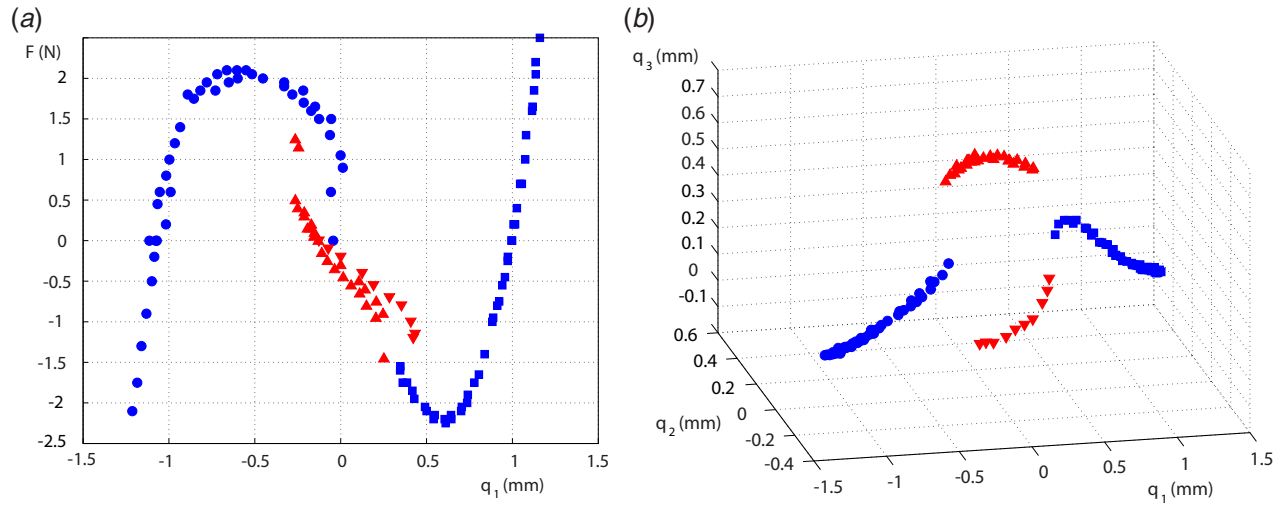

Fig. 11 Deflection as a function of probe force, moderately-buckled: (*a*) projected onto shape 1 and (*b*) a 3D rendition of the three shapes changing under load

on a large-scale shaker and subject to a harmonic excitation of magnitude 2.45 g at a frequency of 100 Hz. Dynamic DIC

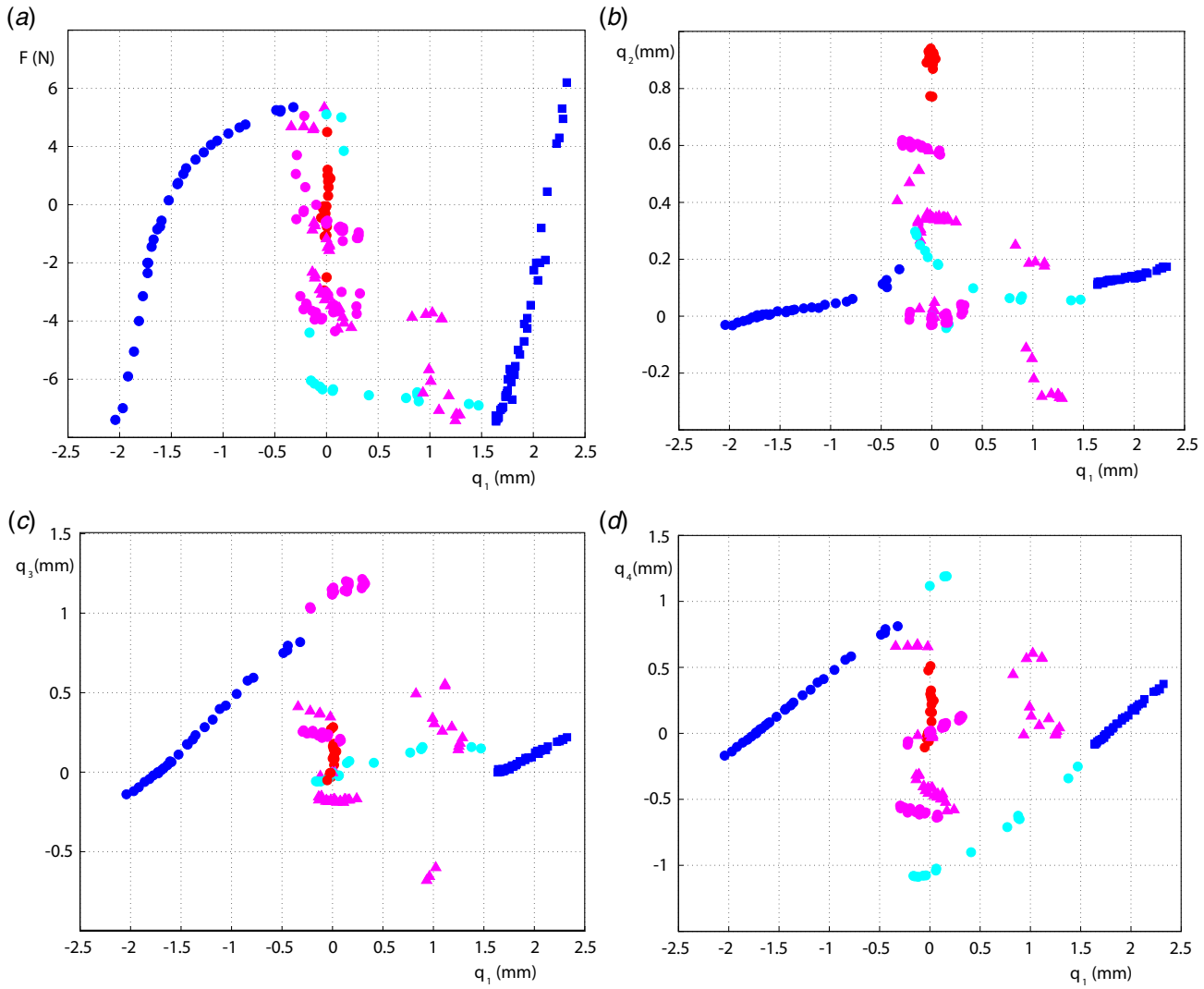

Fig. 12 Examination of panel deformation projected onto the buckled shapes: (*a*) deflection as a function of probe force projected onto shape 1, (*b*) projected deflection of shape 1 versus shape 2, (*c*) versus shape 3, and (*d*) versus shape 4 (Color version online.)

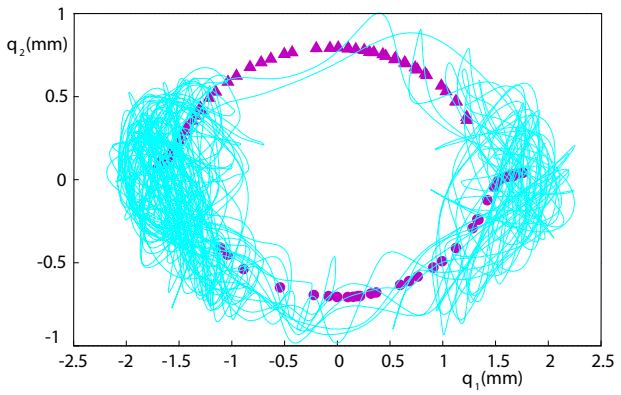

Fig. 13 Dynamic trajectories indicating persistent but erratic snap-through, superimposed on the underlying static probing behavior

(sampling at a frame rate of 5000 Hz) was then used to measure the panel motion and plotted in terms of the first two buckled modes, the trajectories are shown superimposed on the static probing results in Fig. 13.

The trajectories are not surprisingly heavily influenced by the two co-existing stable equilibria (the initial buckled shape and its inverted near mirror-image, with central amplitude of a little less than 2 mm), but we also see the influence of the asymmetric paths taken by the trajectories in the transitions—despite the fact that the static load was applied as a point load at the center and the effective inertial loading is distributed. The preferred paths (both statically and dynamically) can be viewed as energetically favorable valleys in a potential energy landscape.

A final result from dynamic testing is shown in Fig. 14, in terms of typical times series, in which the data from three discrete locations along the panel centerline have been superimposed. Specifically, the blue data (Y_{frame}) were the motion of the frame, the red data were taken from the quarter point Y_A, and the green data correspond to the lateral motion at the center of the plate Y_B, snapping erratically between the underlying stable equilibria.

Here, the system is subject to a ramped loading, i.e., the excitation is still single frequency but now the magnitude is slowly ramped from 1 g to 4 g. After a very brief transient (starting from the shaker being switched on), we initially observe a gradually increasing, predominantly harmonic, response. When the magnitude reaches approximately 2 g (after about 11 s), the motion starts to exhibit erratic, nonlinear behavior, quickly followed by snap-through (after about 13 s), bringing with it serious implications for fatigue. The form of these oscillations are familiar from the study of chaotic behavior in other similarly bi-stable systems [5,26].

If we take the final 15 s of the time series from Fig. 14 for Y_B, we observe persistent snap-through. This is shown in Fig. 15(*a*), and although this is mildly non-stationary due to the slow ramp in force magnitude, the behavior exhibits the main features of chaos, i.e., an erratic random-like response. The underlying influence of the stable equilibria (shown as the grey/red dashed lines) is apparent. Figure 15(*b*) shows a histogram that reflects the time the trajectory spends in certain values of Y_B, binned into one hundred divisions. In this way we see that the trajectory dwells (oscillates) in the vicinity of the stable equilibria at $Y_B \approx 0$ mm and $Y_B \approx 4$ mm and tends to pass relatively quickly between them. Even though the velocity was not measured, the rate of change of position can be studied with the use of time-lag embedding [27]. This technique involves plotting a measured variable against delayed versions of itself as a proxy for velocity. Figure 15(*c*) shows how plotting the time series against itself but delayed by Δt produces a pseudo phase projection. Since the forcing frequency is 100 Hz, and the sampling rate is 5000 Hz, a delay of 10 time-steps was chosen as a suitable value, i.e., a fifth of the forcing period, and we obtain a useful plot of the erratic snap-through behavior that is topologically equivalent to a conventional position-velocity phase projection. The relatively severe snapping behavior (compared with small amplitude periodic behavior) has clear implications for fatigue, and the sudden onset of this type of behavior suggests a threshold that would be crucial to know in practice.

6 Discussion

Nonlinear structures are capable of exhibiting a variety of co-existing equilibrium configurations under nominally fixed (force and boundary) conditions. This is especially true in a typical post-buckled scenario. Under the quasi-static increase in axial loading a structure will (elastically) deflect into energetically favorable states along an equilibrium *path*. Under a reversal of loading direction, the system may, or may not, follow the original path: hysteresis may occur. Also, the paths may not be continuous and sudden dynamic jumps occur [28–32]. However, it is only possible to follow one path at a time. Any remote equilibrium

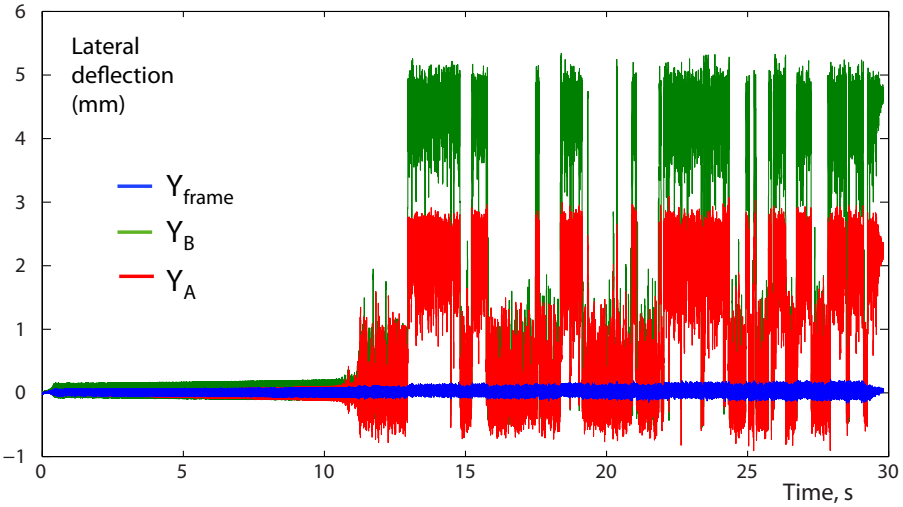

Fig. 14 Displacement time series (three representative locations) under ramped excitation culminating in chaotic snap-through behavior. The displacement is measured from one of the initial stable equilibrium states.

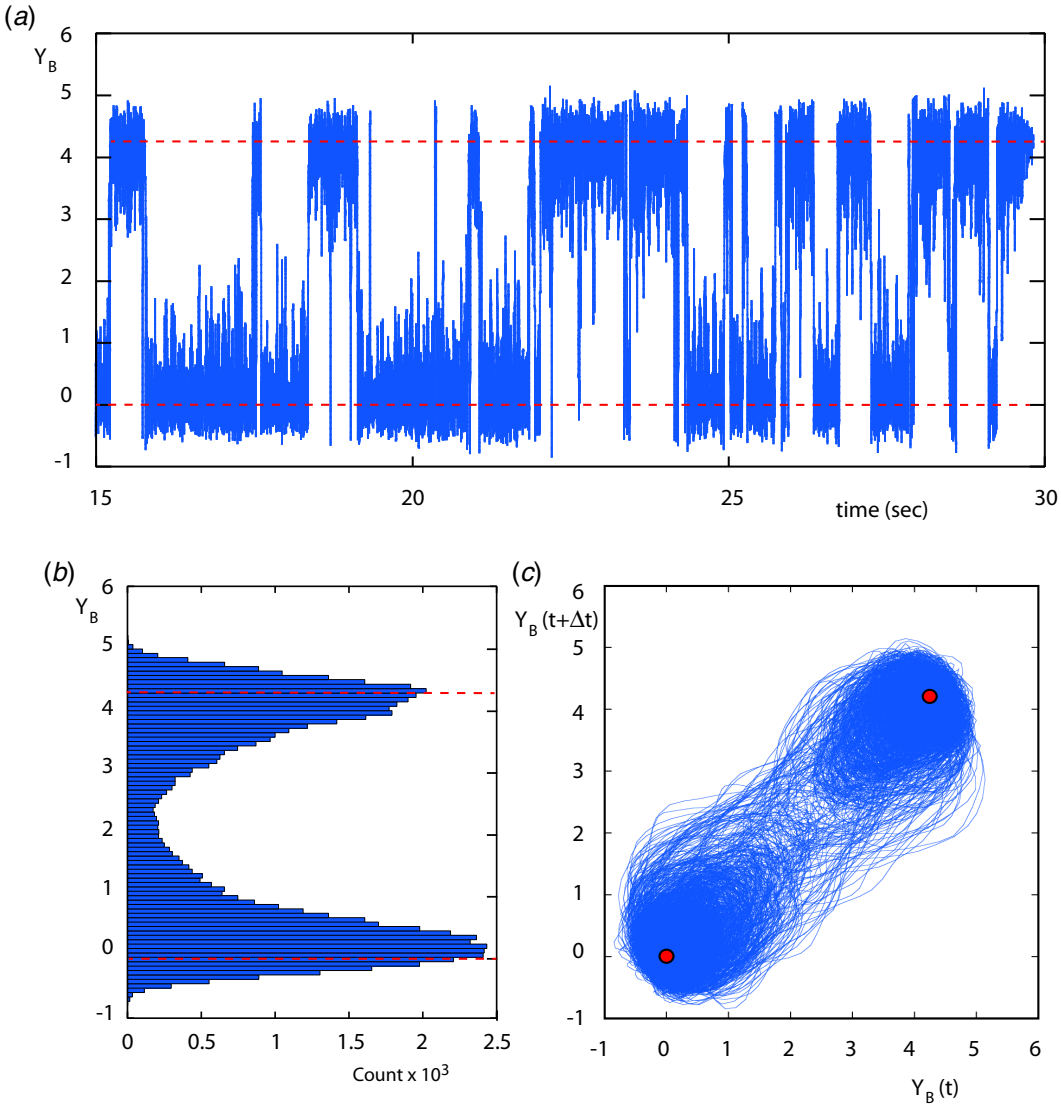

Fig. 15 (*a*) A measured time series taken for the center of panel 1, (*b*) histogram of the trajectory position, and (*c*) a reconstructed phase projection using time-lag embedding

configurations can typically only be accessed using large perturbations or via a special loading history. Exploiting lateral probing (using a displacement-controlled point force) is used here to identify certain otherwise unstable equilibria, for example, when the probe force drops to zero, and provide a more detailed summary of equilibrium configurations. A complete picture would require multiple force (and torque) probes [9] commensurate with the higher-order space in which the system evolves, i.e., essentially an actuator for every generalized coordinate. The DIC system allows a full-field displacement description while recognizing the limited constraint location of the probe (a point force applied at the panel center). However, this general approach provides a window into the equilibrium configuration space of a nonlinear structure.

7 Conclusions

This paper described a set of experiments in which slender, buckled rectangular panels are subject to lateral probing in the form of a displacement-controlled central point force. Measuring the full-field deflection of the panel, as a function of the applied (probe) force, sheds light on possible equilibrium configurations including "free" equilibria when the applied force drops to zero. The central constraint then allows a deeper exploration of multiple equilibrium paths and the transition between co-existing equilibria. The thin panels were made of aluminum, with two sets of boundary conditions, with the spatial complexity made clear by the use of DIC, and are representative of components commonly used in aerospace applications.

Acknowledgment

This work was supported by the UTC under award number FA8650-16-C-2643, and the NSF under award number CMMI-1926672.

Conflict of Interest

There are no conflicts of interest.

Data Availability Statement

The datasets generated and supporting the findings of this article are obtainable from the corresponding author upon reasonable request.

Appendix: Some Approximate Analysis of the Initial Shapes

Given the geometric similarity of panel 1 to a wide beam, it seems reasonable to appeal to small deflection beam theory in order to provide a rough guide to lateral deflection resulting from a lateral point load, i.e., $\delta = F_0\ L^3/(192\ EI)$, in which δ is the central lateral deflection (and $\equiv Y_B$), F_0 is the lateral load, $L \equiv a$ is the longitudinal span (in the clamped-to-clamped direction), E is Young's modulus, $I = bd^3/12$ is the second moment of area for a rectangular cross-section of width b and thickness d. However, since this is not a strictly 1D structural component, it seems reasonable (and suggested in Ref. [33]) to include a correction associated with anti-clastic bending and replace E by $E/(1-\nu^2)$, where ν is the Poisson's ratio (taken as 0.33), and thus $\delta = 0.0557F_0a^3/(Ebd^3)$, and for $a/b = 1.8$, we get $\delta = 0.1F_0a^2/Ed^3$.

Prior to clamping, in addition to in-plane sliding, the (loose) boundary conditions would allow a little rotation along the edges, and the central deflection under a central point load *with simply supported boundary conditions* is given by $F_0\ L^3/(48EI)$, i.e., a quarter as stiff, all other things being equal. We might therefore expect the post-buckled central deflection to depend on the lateral push load somewhere between these two values, but closer to the former. Furthermore, the in-plane boundary conditions are assumed to provide no resistance (i.e., sliders, until after clamping has taken place). These relations are used as a guide in order to provide a reasonable proxy for the *extent* of the post-buckling, with actual deflections measured accurately using DIC.

In the experiments described in this paper, the buckled central deflection was on the order of a few millimeters, and hence, $\delta_c/d \approx 1 \rightarrow 10$, which is not necessarily considered small. In the cases with larger deflection, it is more appropriate to estimate a lateral force-deflection relation based on large deflection theory [16]. For the purposes of this study, we simply state that this is a hardening spring effect, and despite the allowance for in-plane edge movement, it means that the approximate forces used to cause an initial buckle result in somewhat smaller deflections than the linear theory suggests.

For panel 2 (clamped on all four sides), we can also appeal to analysis but this time the boundary conditions require the use of (thin, small deflection) plate theory incorporating all four boundary conditions and the aspect ratio of the panel. In this case, the central lateral deflection is given in Ref. [16] as $\delta = 0.0067F_0a^2/D$ (specifically for $a/b = 1.286$), and since $D = Ed^3/12(1-\nu^2)$, we get $\delta = 0.0716\ F_0a^2/(Ed^3)$. We see that clamping the two free sides results in less deflection, and thus an increase in linear stiffness as compared to panel 1, although they have different aspect ratios. For *square* panels, the additional clamped edges provide a roughly 36% increase in stiffness over the wide-beam panel with a central point load, based on plate theory and confirmed by FEA (using ABAQUS). The same comments mentioned above about large deflections also apply to this case.

References

[1] Spottswood, S. M., Beberniss, T. J., Eason, T. G., Perez, R. A., Donbar, J. M., Ehrhardt, D. A., and Riley, Z. B., 2019, "Exploring the Response of a Thin, Flexible Panel to Shock-Turbulent Boundary-Layer Interactions," J. Sound. Vib., **443**, pp. 74–89.

[2] Virgin, L. N., 2007, *Vibration of Axially-Loaded Structures*, Cambridge University Press, New York.

[3] Timoshenko, S. P., and Gere, J., 1961, *Theory of Elastic Stability*, Dover, New York.

[4] Thompson, J. M. T., and Hunt, G. W., 1984, *Elastic Instability Phenomena*, Wiley, Chicester.

[5] Wiebe, R., and Virgin, L. N., 2016, "On the Experimental Identification of Unstable Static Equilibria," Proc. R. Soc. London A: Math., Phys. Eng. Sci., **472**(20160172), pp. 1–15.

[6] Thompson, J. M. T., Hutchinson, J. W., and Sieber, J., 2017, "Probing Shells Against Buckling: A Non-Destructive Technique for Laboratory Testing," Int. J. Bifurcat. Chaos, **27**(14), p. 1730048.

[7] Neville, R. M., Groh, R. M. J., Pirrera, A., and Schenk, M., 2018, "Shape Control for Experimental Continuation," Phys. Rev. Lett., **120**, p. 254101.

[8] Ross, S. D., Bozorgmagham, A. E., Naik, S., and Virgin, L. N., 2018, "Experimental Validation of Phase Space Conduits of Transition Between Potential Wells," Phys. Rev. E, **98**, p. 052214.

[9] van Iderstein, T., and Wiebe, R., 2018, *Experimental Path Following of Unstable Equilibria for Snap-Through Buckling*, Vol. 1, G. Kerschen, ed., Springer, Cham, pp. 17–22.

[10] Xu, Y., and Virgin, L. N., 2019, "Probing the Force Field to Identify Potential Energy," ASME J. Appl. Mech., **86**(10), p. 101008.

[11] Stoll, F., 1994, "Analysis of the Snap Phenomenon in Buckled Plates," Int. J. Non-Linear Mech., **29**(2), pp. 123–138.

[12] Bryan, G. H., 1891, "On the Stability of a Plane Plate Under Thrust in Its Own Plane with Application to the Buckling of the Side of a Ship," Proc. London Math. Soc., **22**(1), pp. 54–67.

[13] Levy, S., Bending of rectangular plates with large deflections. Technical report, NASA Report 737, 1942.

[14] Coan, J. M., 1951, "Large Deflection Theory for Plates With Small Initial Curvature Loaded in Edge Compression," Trans. ASME, **73**, pp. 143–151.

[15] Yamaki, N., 1959, "The Post-Buckling Behaviour of Rectangular Plates With Small Initial Curvature Loaded in Edge Compression," ASME J. Appl. Mech., **26**(2), pp. 407–414.

[16] Timoshenko, S. P., and Woinowsky-Krieger, S., 1959, *Theory of Plates and Shells*, McGraw-Hill, New York.

[17] Sundara Raja Iyengar, K. T., and Matin Naqvi, M., 1966, "Large Deflections of Rectangular Plates," Int. J. Non-Linear Mech., **1**(2), pp. 109–122.

[18] Bulson, P. S., 1970, *The Stability of Flats Plates*, Chatto and Windus, London.

[19] Walker, A. C., 1984, "*A Brief Review of Plate Buckling Research*," *Behaviour of Thin-walled Structures*, Rhodes, J., and Spence, J., eds., Elsevier.

[20] Ugural, A. C., 1999, *Stresses in Plates and Shells*, McGraw-Hill, New York.

[21] Ng, C. F., 1989, "Nonlinear and Snap-through Responses of Curved Panels to Intense Acosutic Excitation," J. Air., **26**(3), pp. 281.

[22] Blevins, R. D., Holehouse, I., and Wentz, K. R., 1993, "Thermoacosutic Loads and Fatigue of Hypersonic Vehicle Skin Panels," J. Air., **30**(6), pp. 971–978.

[23] Dhainaut, J. M., Mei, C., Spottswood, S. M., and Wolfe, H. F., 2002, "Sonic Fatigue Design and Nonlinear Panel Response to Flight Nonwhite Pressure Fluctuations," 43rd AIAA/ASME/ASCE/AHS/ASC Structures, Structural Dynamics, and Materials Conference, Denver, CO, April.

[24] Gordon, R. W., and Hollkamp, J. J., 2006, "Nonlinear Random Response of a Clamped Plate: a Well-characterized Experiment," 47th AIAA/ASME/ASCE/AHS/ASC Structures, Structural Dynamics, and Materials Conference, Newport, RI, May.

[25] Cui, D., and Hu, H., 2014, "Thermal Buckling and Natural Vibration of a Rectangular Thin Plate with in-plane Stick-slip-stop Boundaries," J. Vib. Control, **22**(7), pp. 1950–1966.

[26] Murphy, K. D., Virgin, L. N., and Rizzi, S. A., 1996, "Experimental Snap-through Boundaries for Acoustically Excited, Thermally Buckled Plates," Exp. Mech., **36**, pp. 312–317.

[27] Virgin, L. N., 2000, *Introduction to Experimental Nonlinear Dynamics*, Cambridge University Press, Cambridge UK.

[28] Stein, M., Loads and deformation of buckled rectangular plates. Technical report, NASA Technical Report R-40, 1959.

[29] Chen, H., and Virgin, L. N., 2006, "Finite Element Analysis of Postbuckling Dynamics in Plates: Part I: An Asymptotic Approach," Int. J. Solids. Struct., **43**(13), pp. 3983–4007.

[30] Schaeffer, D., and Golubitsky, M., 1979, "Boundary Conditions and Mode Jumping in the Buckling of a Rectangular Plate," Commun. Math. Phys., **69**, pp. 209–236.

[31] Chen, H., and Virgin, L. N., 2006, "Finite Element Analysis of Postbuckling Dynamics in Plates: Part II: A Nonstationary Analysis," Int. J. Solids. Struct., **43**(13), pp. 4008–4027.

[32] Taffetani, M., Jiang, X., Holmes, D. P., and Vella, D., 2018, "Static Bistability of Spherical Caps," Proc. R. Soc. A, **474**(2213).

[33] Young, W., and Bufynas, R., 2011, *Roark's Formulas for Stress and Strain*, McGraw-Hill.